AIAA JOURNAL
Vol. 50, No. 5, May 2012

Dynamics and Performance of Tailless Micro Aerial Vehicle with Flexible Articulated Wings

Aditya A. Paranjape,* Soon-Jo Chung,† and Harry H. Hilton‡
University of Illinois at Urbana–Champaign, Urbana, Illinois 61801
and
Animesh Chakravarthy§
Wichita State University, Wichita, Kansas 67260

DOI: 10.2514/1.J051447

The purpose of this paper is to analyze and discuss the performance and stability of a tailless micro aerial vehicle with flexible articulated wings. The dihedral angles can be varied symmetrically on both wings to control the aircraft speed independently of the angle of attack and flight-path angle, while an asymmetric dihedral setting can be used to control yaw in the absence of a vertical tail. A nonlinear aeroelastic model is derived, and it is used to study the steady-state performance and flight stability of the micro aerial vehicle. The concept of the effective dihedral is introduced, which allows for a unified treatment of rigid and flexible wing aircraft. It also identifies the amount of elasticity that is necessary to obtain tangible performance benefits over a rigid wing. The feasibility of using axial tension to stiffen the wing is discussed, and, at least in the context of a linear model, it is shown that adding axial tension is effective but undesirable. The turning performance of an micro aerial vehicle with flexible wings is compared to an otherwise identical micro aerial vehicle with rigid wings. The wing dihedral alone can be varied asymmetrically to perform rapid turns and regulate sideslip. The maximum attainable turn rate for a given elevator setting, however, does not increase unless antisymmetric wing twisting is employed.

Nomenclature

b, c	=	wing span and chord length
D, L, Y	=	drag, lift, and side force
E, G	=	Young's modulus and modulus of rigidity of a material
I_b, I_p, $\tilde{J}$	=	second moment of area about the in-plane axis along the direction of bending, polar moment of area, and torsional stiffness of a cross section of the wing
$\mathbf{J}_R$, $\mathbf{J}_L$, $\mathbf{J}$	=	moment of inertia tensor of the right and left wings and the aircraft body, respectively, in the aircraft body frame
$\mathbf{J}_s$	=	second moment of area of a cross section with components in the local wing station frame
$\tilde{m}_R$, $\tilde{m}_L$, m	=	mass per unit span of the right and left wings, total mass of aircraft
$\mathbf{r}_{\mathrm{CG}}$	=	position vector of the aircraft center of gravity
$S(\mathbf{p})\mathbf{q}$	=	cross product $\mathbf{p} \times \mathbf{q}$, $\mathbf{p}, \mathbf{q} \in R^3$
T	=	axial tension in the wing
$\mathbf{T}_{FG}$	=	rotation matrix from frame G to frame F
$\mathbf{u}_B = [u \quad v \quad w]$	=	body axis aircraft wind velocity components
$\mathbf{u}_f = [0 \quad 0 \quad \dot{\xi}_f]$	=	rate of change of bending displacement ξ_f in the local wing frame
$\mathbf{V}(y)$, $V(y)$, V_∞	=	local wind velocity vector, local wind speed, freestream speed
X, Y, Z	=	position of the aircraft in the ground frame
X_A, Y_A, Z_A	=	body frame components of the aerodynamic force per unit span
X_B, Y_B, Z_B	=	body frame components of the net aerodynamic and gravitational forces
x_a, x_e	=	distance of aerodynamic center and center of gravity from the twist axis at a given station along the wing span, normalized with respect to c
α, β	=	angle of attack and sideslip
β_R, β_L	=	sweep angle of right and left wing
γ, χ	=	flight-path angle, wind axis heading angle
δ_R, δ_L	=	right and left wing dihedral angles
θ_R, θ_L, θ_a	=	right and left wing root twist angles, antisymmetric wing twist, $\theta_R = -\theta_L$
$\theta_s(y)$	=	sectional wing twist from wing flexibility
ν	=	distance of flow separation point from the leading edge, measured along the wing chord
ρ_w	=	density of the wing
ϕ, θ, ψ	=	Euler angles
ω	=	turn rate ($\dot{\chi}$)
$\boldsymbol{\omega}_B = [p \quad q \quad r]^T$	=	angular velocity of the airframe, body axis components (roll, pitch, yaw)
$\boldsymbol{\omega}_R$, $\boldsymbol{\omega}_L$	=	angular velocity of the wings about the root, body axis components
$\boldsymbol{\omega}_s = [0 \quad \dot{\theta}_s \quad 0]$	=	twist rate of a wing station, components in the wing station frame

Subscripts

B	=	body
R	=	wing root (used to denote a coordinate axis frame situated at the wing root)
s	=	wing station

Presented as Paper 2010-7937 at the AIAA Atmospheric Flight Mechanics Conference, Toronto, Ontario, 2–5 August 2010; received 21 June 2011; revision received 13 September 2011; accepted for publication 4 November 2011.

*Doctoral Candidate, Department of Aerospace Engineering; paranja2@illinois.edu. Student Member AIAA.
†Assistant Professor, Department of Aerospace Engineering; sjchung@illinois.edu. Senior Member AIAA.
‡Professor Emeritus, Department of Aerospace Engineering; h-hilton@illinois.edu. Fellow AIAA.
§Assistant Professor, Department of Aerospace Engineering; animesh.chakravarthy@wichita.edu. Senior Member AIAA.

I. Introduction

THE present paper is intended to contribute toward the broader problem of developing a flapping wing micro aerial vehicle (MAV) capable of agile flight in constrained environments. This paper significantly extends the recent results of [1], which investigated the performance, stability, and controllability of a tailless aircraft with rigid articulated wings. Birds are natural role models for designing tailless MAVs, wherein the aforementioned attributes can be engineered. MAVs typically fly in the range of 2–20 m/s, and in a Reynolds number range of 1×10^3–1×10^5, which coincides with that of the birds. Therefore, it is worth investigating the mechanics of avian flight and making an attempt to reverse engineer them. Conversely, a study of the flight mechanics of MAVs can shed light on several aspects of bird flight.

Figure 1 shows a schematic of one such MAV concept inspired by small birds such as the barn swallow. It would lack a vertical tail and, instead, use the wing dihedral and twist effectively for control. Complex maneuvers require a combination of open- and closed-loop capabilities. However, since the performance achievable in the closed loop (with control and guidance) is contingent upon the limitations of the airframe, it is necessary to evaluate the (open-loop) performance and stability of the aircraft itself.

a) Tailless articulated wing aircraft concept

b) Barn swallow

Fig. 1 A schematic showing a tailless aircraft concept with flexible wings. This aircraft is motivated by small, agile birds like the barn swallow shown on the right [http://commons.wikimedia.org/wiki/File:Barn_swallow_6909.jpg (retrieved 3 Feb. 2012)].

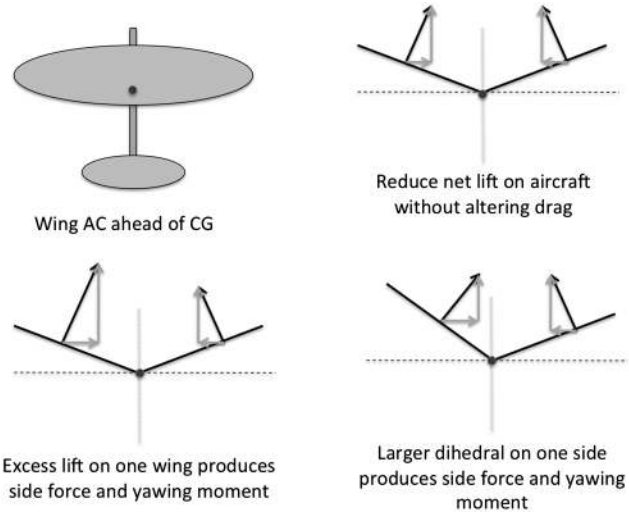

Fig. 2 A schematic depicting the use of wing dihedral for longitudinal and yaw control [1].

Chung and Dorothy [2] studied a neurobiologically inspired controller for flapping flight and demonstrated it on a robotic testbed. Their controller, similar to avian flight, could switch between flapping and gliding flight smoothly using coupled Hopf oscillators. The present paper is concerned with the performance and stability during gliding flight, whereas work is currently in progress in parallel for the flapping phase. A separate analysis of the two flight phases would yield a complete picture of the dynamics of flapping flight, its performance capabilities, and limitations, and create a solid foundation for control design [2,3].

There is considerable interest in morphing wing aircraft where the wing geometry can be optimized during the different stages of its mission. One approach to using dynamic morphing for control actuation is to use highly flexible articulated wings. Wing articulation is naturally built into flapping wing aircraft and therefore, it is of interest to probe its control and maneuvering capability. Flexible wings are usually lighter than geometrically similar rigid wings, and flexibility acts as a natural actuation amplifier. However, flexible wings may need additional stabilizers to prevent divergence and flutter if any of the missions take the aircraft into the respective speed regimes [4,5]. MAVs are usually designed to fly at relatively slower speeds, and hence it is reasonable to expect that a large degree of flexibility can be safely introduced without risking aeroelastic instability. At the same time, aeroelastic analyses can be computationally intensive. It is of interest, therefore, to compare rigid and flexible wings in order to determine how far an analysis based on rigid wings, which is relatively simpler, is applicable to flexible wings.

A. Literature Review

It is rather obvious how wing twist can be used for roll control and high-lift generation. The idea of using an asymmetric dihedral for yaw control can be traced to a recent paper by Bourdin et al. [6]. Tran and Lind [7] examined the stability of a flexible wing aircraft for various wing deflection configurations. Paranjape et al. [1] derived a flight dynamic model of articulated wing aircraft and used bifurcation and continuation methods to study the benefits and limitations of wing articulation for yaw control (Fig. 2 shows how the wing dihedral angles can be used for control). They concluded that the wing dihedral alone provides sufficient yaw control for trim, but also noted that the sign of the yaw control effectiveness changes as a function of the angle of attack and angular rates. Control laws for stabilizing and maneuvering an articulated wing aircraft have been presented in [3,8]. A roll control mechanism was demonstrated by Stanford et al. [9] for an aircraft equipped with highly flexible membrane wings.

A variety of aircraft models incorporating wing and fuselage flexibility have been proposed in the literature, although most of these models do not consider wing articulation. Waszak and Schmidt [10] derived a complete nonlinear model of an aircraft with flexible wings. Their aerodynamic model, however, assumed a steady flow, and their frame of reference consisted of the so-called mean axes which are hard to locate in a practical situation. Meirovitch and Tuzcu [11] extended their model in several ways: they used a more intuitive reference frame (the conventional body axes) and a more accurate Theodorsen's unsteady aerodynamics theory for computing the forces and moments [12]. Recently, Nguyen and Tuzcu [13] presented a dynamic model for a fully flexible aircraft. These papers worked with a small strain, small displacement beam theory. In contrast, Patil and Hodges [14] and Raghavan and Patil [15] derived a geometrically exact (large displacement) small strain nonlinear beam model and used it to study the dynamics and stability of flying wings. Shearer and Cesnik [16] and Su and Cesnik [17] used nonlinear flight dynamic and structural models to investigate the effects of structural nonlinearities on the dynamic stability of aircraft characterized by large aspect ratio wings and blended wing–body configurations, respectively. Baghdadi et al. [18] used bifurcation analysis to study

the performance and stability of a flexible aircraft model based on [10] and concluded that flexibility must be accounted for carefully during the control design process. They also noted demonstrated that a control law designed assuming a rigid configuration could trigger instabilities in an otherwise identical aircraft with flexible wings. Rodden [19] derived analytical expressions, backed by experimental approximations, for increments in the rolling moment derivatives arising from aeroelastic effects.

B. Main Contributions

Broadly, the present paper is meant to be a sequel to [1]. Unlike the prior work referenced previously, the present paper is concerned with the stability as well as performance of an MAV with flexible articulated wings. The objective is to explain the underlying physics to lay the foundation for a sound control design. Toward that objective, select performance metrics and stability of the MAV in [1] are compared with those of a similar MAV equipped with flexible wings. The purpose of this exercise is twofold. First, it helps to identify the benefits of using wing flexibility. Second, and less obviously, it helps to identify the extent to which a rigid MAV model can accurately capture the dynamics of a flexible wing MAV. The flight dynamics will be rendered unstable if the wing is structurally unstable. On the other hand, if the structural stability of the wing can be guaranteed, then the performance and stability of the motion can be computed reliably by considering "macroscopic" parameters like the resultant forces which depend on the shape, rather than stability, of the wing. Therefore, an analysis like that in the present paper would depend largely on the wing geometry (which is usually well known a priori) rather than a precise knowledge of the elastic parameters.

The specific questions answered in this paper include the following:

1) For the wing size of a typical bird-sized MAV, what value of Young's modulus (E) should the wing have in order for the MAV to offer a significant performance improvement over a rigid wing MAV? Equivalently, until what point is the open-loop analysis of a rigid aircraft relevant to a flexible winged aircraft? The notion of the effective dihedral is introduced in a bid to answer these questions.

2) A stiff wing may be required for certain maneuvers. Axial tension in the wing is an intuitive stiffener. How effective and useful is it? We answer this question in the negative: it is effective, but of limited use.

3) How is the stability of the motion altered in the presence of flexible wings? The wings are assumed to be quasi-statically deformed and therefore the structural dynamics of the wings have no bearing on the conclusion. In other words, the wing is assumed to be structurally stable and its dynamics sufficiently faster than the aircraft.

4) Is there a measurable improvement in the steady-state turning performance? Steady-state turn rate is the only agility metric which is based entirely on a steady maneuver [20]. It is also an important benchmark to evaluate the efficacy of a yaw control mechanism.

A complete nonlinear dynamic model for an aircraft with flexible, articulated wings is derived in the paper. The wings are assumed to be linearly elastic and the Euler–Bernoulli beam model is used for modeling wing deformation under aerodynamic loading. The linear model can be replaced readily with a nonlinear deformation model [14] in the coordinate systems proposed in this paper. The variation in the position of the center of gravity (CG) due to wing motion is incorporated in the model. The lift model proposed for deriving the aerodynamic forces and moments, originally proposed by Goman and Khrabrov [21], is an unsteady model which is valid at high angles of attack. The dynamic model derived in this paper can be used to analyze flapping flight of aircraft which fly at Reynolds numbers of $\mathcal{O}(1 \times 10^4)$ and higher. The limit on the Reynolds number arises from the fact that, at lower Reynolds numbers, delayed stall effects, leading-edge vortices, and wake capture provide a significant portion of the lift [22]. These effects are not captured within the ambit of the model proposed in this paper. The present model may be viewed as an extension of the models in [2,23,24] in that it uses a strip theory-based scheme for computing the net aerodynamic force on the wings and horizontal tail and treats each wing as a single (flexible) body unlike the multiple-rigid-body model proposed in [7,25].

A bifurcation analysis [26] of turning flight is performed assuming quasi-statically deformed wings to identify the nature of the instabilities, and the performance and control deflections are compared with those of a rigid winged aircraft. Bifurcation analysis of turning flight demonstrates two salient features of a flexible winged aircraft. First, wing flexibility reduces the amount of sideslip encountered in turns controlled by wing twist, while simultaneously increasing the turn rate substantially. Second, and less obviously, the maximum achievable turn rate with zero sideslip is actually reduced due to wing flexibility. This happens because of two reasons. First, the yawing moment due to wing dihedral peaks when the dihedral angle is ± 45 deg. Second, the wing twist that arises from flexibility causes the aircraft to fly at a slower speed for a given horizontal tail setting than it would have had the wing been rigid. The performance limitations of aircraft with small to moderate aspect ratio flexible wings may be reliably computed assuming that the wings are rigid, thereby greatly reducing the modeling and computational difficulty in the process. This reduction does not apply to the assessment of stability.

This paper is organized as follows. The equations of motion are derived in Sec. II. The concept of the effective dihedral is introduced in Sec. III, and the role played by the effective dihedral in designing the elastic modulus of the wing is described. The effect of axial tension on the effective dihedral is analyzed. Specifically, the bifurcation analysis of a steady turn is described in Sec. III.D.

II. Differential Equations

The dynamic model derived in this section is general enough that it can be applied to a wider class of problems, such as flapping and a complete aeroelastic analysis of aircraft.

A. Notation

Capital letters are reserved for forces, matrices, and for denoting coordinate frames. Small letters are used for scalars when not in bold, and for vectors when used with bold font. Given a vector $\mathbf{x} \in \mathbb{R}^3$, $S(\mathbf{x})$ denotes the cross product operator; i.e., for any two vectors $\mathbf{x}, \ \mathbf{y} \in \mathbb{R}^3$, $S(\mathbf{x})\mathbf{y} \triangleq \mathbf{x} \times \mathbf{y}$. Similarly, $S^2(\mathbf{x})\mathbf{y} = S(\mathbf{x})[S(\mathbf{x})\mathbf{y}] = \mathbf{x} \times (\mathbf{x} \times \mathbf{y})$. Given a variable $p(t, y)$, its time derivative is denoted by $\dot{p}(t, y) \triangleq \partial p(t, y)/\partial t$. Its spatial derivative is denoted by $p'(t, y) \triangleq \partial p(t, y)/\partial y$. Note that when $p(t, y) \equiv p(t)$, $\dot{p}(t) = \mathrm{d}p(t)/\mathrm{d}t$.

B. Coordinate Frames of Reference

Given frames F and G, the matrix $\mathbf{T}_{FG}$ is a rotation matrix which transforms the components of a vector from the G frame to F. The body frame, denoted by B, is attached to the body with the x-z plane coincident with the aircraft plane of symmetry when the wings are undeflected. The x axis points toward the aircraft nose. The z axis points downwards, and the y is defined to create a right-handed coordinate system.

Consider the frame R based at the right wing root. Its origin coincides with that of the B frame, which is akin to neglecting the fuselage width. This assumption does not alter the rotation matrices in any way. The frame R is related to the B frame via three rotations at the wing root: a sweep rotation β_R about the z axis, followed by a dihedral rotation δ_R about the "$-x$" axis, and a rotation θ_R about the y axis. The y axis points along the wing elastic axis. Thus,

$$\mathbf{T}_{BR} = \begin{bmatrix} \cos\beta_R & -\sin\beta_R & 0 \\ \sin\beta_R & \cos\beta_R & 0 \\ 0 & 0 & 1 \end{bmatrix} \begin{bmatrix} 1 & 0 & 0 \\ 0 & \cos\delta_R & \sin\delta_R \\ 0 & -\sin\delta_R & \cos\delta_R \end{bmatrix} \times \begin{bmatrix} \cos\theta_R & 0 & \sin\theta_R \\ 0 & 1 & 0 \\ -\sin\theta_R & 0 & \cos\theta_R \end{bmatrix} \tag{1}$$

A similar matrix can be defined for the left wing. The matrix $\mathbf{T}_{BR}$ is introduced here in the most general form, i.e., no rotation is ignored, which makes it applicable to flapping flight dynamics. However, the analysis in Sec. III assumes that $\beta_R = \beta_L = 0$.

The frame $S \equiv S(y)$ is the frame located at a spanwise wing station with origin at the elastic center and y axis pointing along the elastic axis. The frame S is related to R via two rotations: a rotation about the x axis through the strain $\xi'_f(y)$ and a rotation (twist) $\theta_s(y)$ about the y axis. Thus,

$$\mathbf{T}_{RS} = \begin{bmatrix} \cos\theta_s(y) & 0 & \sin\theta_s(y) \\ \sin[\xi'_f(y)]\sin\theta_s(y) & \cos[\xi'_f(y)] & -\sin[\xi'_f(y)]\cos\theta_s(y) \\ -\cos[\xi'_f(y)]\sin\theta_s(y) & \sin[\xi'_f(y)] & \cos[\xi'_f(y)]\cos\theta_s(y) \end{bmatrix} \tag{2}$$

In the interest of analytical tractability, for the purpose of computing the velocities and acceleration terms, it will be assumed that $\mathbf{T}_{BS} = \mathbf{T}_{BR}$, i.e., the deformations are small enough that they do not alter the coordinate transformations. However, in Sec. II.G, this assumption is relaxed for computing the aerodynamic forces and moments. This is the primary source of the difference in the forces and moments produced by rigid and flexible wings.

C. Calculating the Velocity at a Spanwise Station

The angular velocity of the right wing, $\boldsymbol{\omega}_R$ with components in the body frame, is given by

$$\boldsymbol{\omega}_R = \begin{bmatrix} -\cos\beta_R & -\cos\delta_R\sin\beta_R & 0 \\ -\sin\beta_R & \cos\delta_R\cos\beta_R & 0 \\ 0 & \sin\delta_R & 1 \end{bmatrix} \begin{bmatrix} \dot{\delta}_R \\ \dot{\theta}_R \\ \dot{\beta}_R \end{bmatrix} \tag{3}$$

It is calculated using a 3-1-2 Euler angle sequence which is also used to calculate $\mathbf{T}_{BR}$. The same sequence can be used to model a flapping wing, in which case the amplitude and phase of the motion corresponding to each degree of freedom need to be prescribed. In contrast, most flapping wing models prefer to identify a stroke plane in which the flapping motion is constrained, and which also contains the twist axis (see [2,22,25] and the references cited therein).

Let $\mathbf{y} = [\,0 \quad y \quad \xi_f\,]^T$ denote the coordinates of a spanwise station on the wing along the twisting axis. Then the local wind velocity, with components in the local station frame, is given by

$$\mathbf{V} = \mathbf{T}_{SB}\mathbf{u}_B + \mathbf{u}_f + \mathbf{T}_{SB}S(\boldsymbol{\omega}_B + \boldsymbol{\omega}_R)\mathbf{T}_{BR}\mathbf{y} \tag{4}$$

A similar expression can be determined for the angular velocity of the left wing at the root, $\boldsymbol{\omega}_L$, and the local velocity at a spanwise station on the left wing.

The aerodynamic center is assumed to be located at the quarter-chord point. The velocity at the three-quarter-chord point of a spanwise station is used for calculating the angle of attack, and it is given by

$$\mathbf{V}_{3/4}(y) = \mathbf{V} + S(\boldsymbol{\omega}_s)\mathbf{x}_{3/4} \tag{5}$$

where $\mathbf{x}_{3/4} = [\,(x_a - 0.5)_c \quad 0 \quad 0\,]^T$. Let $[\,u_{3/4}(y), \quad v_{3/4}(y), \quad w_{3/4}(y)]$ denote the components of $\mathbf{V}_{3/4}$ in the local station frame, and $V_{3/4}$ its magnitude. Then, the local angle of attack and sideslip can be calculated using

$$\tan\alpha(y) = \frac{w_{3/4}}{u_{3/4}}, \qquad \sin\beta(y) = \frac{v_{3/4}}{V_{3/4}} \tag{6}$$

D. Aircraft Equations of Motion

Let m_R and m_L denote the masses of the right wing and left wing, respectively. Let $\tilde{m}_R$ and $\tilde{m}_L$ denote the masses per unit length of the right wing and left wing, respectively. Let $\mathbf{r}_{\mathrm{CG}}$ denote the position of the CG of the aircraft. Let $\mathbf{r}_s = [x_e c, 0, 0]^T$ denote the location of the CG with respect to the wing twisting axis, and let $\mathbf{y} = [x_e c\cos\theta_s(y), y, \xi_f - x_e c\sin\theta_s(y)]^T$ denote the position of the CG of a wing station in the wing root frame. Let $\boldsymbol{\omega}_s \triangleq [\,0 \quad \dot{\theta}_s \quad 0\,]^T$ denote the angular velocity of a given wing station due to twisting. The total linear momentum of the aircraft is the sum of the momenta of the fuselage and the two wings. The momentum and force vectors are written with respect to the body axes, fixed at the wing root. The linear momentum of the aircraft is given by

$$\begin{aligned} \mathbf{p} = {} & m[\mathbf{u}_B + S(\boldsymbol{\omega}_B)\mathbf{r}_{\mathrm{CG}}] + \tilde{m}_R\int_0^{b/2}[S(\boldsymbol{\omega}_R)\mathbf{T}_{BR}\mathbf{y}]\,\mathrm{d}y \\ & + \tilde{m}_L\int_{-b/2}^{0}[S(\boldsymbol{\omega}_L)\mathbf{T}_{BR}\mathbf{y}]\,\mathrm{d}y + \tilde{m}_R\int_0^{b/2}[\mathbf{T}_{BR}\mathbf{u}_f(y) \\ & + \mathbf{T}_{BR}S(\boldsymbol{\omega}_s)\mathbf{r}_s]\,\mathrm{d}y + \tilde{m}_L\int_{-b/2}^{0}[\mathbf{T}_{BS}\mathbf{u}_f(y) \\ & + \mathbf{T}_{BR}S(\boldsymbol{\omega}_s)\mathbf{r}_s]\,\mathrm{d}y \end{aligned} \tag{7}$$

where m is the total mass of the aircraft, including the masses of the fuselage and the horizontal tail. In Eq. (7), it is assumed that the wing has a constant mass per unit span. It must be noted that this assumption is, strictly speaking, not essential for the derivation of the aircraft equations of motion since no spatial derivatives are involved. In the present case, it only serves the purpose of succinctness. Differentiating the right-hand side with time, and setting $(\mathrm{d}\mathbf{p}/\mathrm{d}t) = \mathbf{F}_b$, we get

$$\begin{aligned} & m[\dot{\mathbf{u}}_B + S(\boldsymbol{\omega}_B)\mathbf{u}_B + S(\dot{\boldsymbol{\omega}}_B)\mathbf{r}_{\mathrm{CG}} + S^2(\boldsymbol{\omega}_B)\mathbf{r}_{\mathrm{CG}} + S(\boldsymbol{\omega}_B)\dot{\mathbf{r}}_{\mathrm{CG}}] \\ & + \tilde{m}_R\int_0^{b/2}\{[S(\boldsymbol{\omega}_R + \boldsymbol{\omega}_B)S(\boldsymbol{\omega}_R) + S(\dot{\boldsymbol{\omega}}_R)]\mathbf{T}_{BR}\mathbf{y} \\ & + S(\boldsymbol{\omega}_R)\mathbf{T}_{BR}\mathbf{u}_f\}\,\mathrm{d}y + \tilde{m}_L\int_{-b/2}^{0}\{[S(\boldsymbol{\omega}_L + \boldsymbol{\omega}_B)S(\boldsymbol{\omega}_L) \\ & + S(\dot{\boldsymbol{\omega}}_L)]\mathbf{T}_{BR}\mathbf{y} + S(\boldsymbol{\omega}_L)\mathbf{T}_{BR}\mathbf{u}_f\}\,\mathrm{d}y + \tilde{m}_R\int_0^{b/2}\{\mathbf{T}_{BR}\dot{\mathbf{u}}_f(y) \\ & + S(\boldsymbol{\omega}_B + \boldsymbol{\omega}_R + \mathbf{T}_{BR}\boldsymbol{\omega}_s)\mathbf{T}_{BR}[\mathbf{u}_f + S(\boldsymbol{\omega}_s)\mathbf{r}_s] \\ & + \mathbf{T}_{BR}S(\dot{\boldsymbol{\omega}}_s)\mathbf{r}_s\}\,\mathrm{d}y + \tilde{m}_L\int_{-b/2}^{0}\{\mathbf{T}_{BR}\dot{\mathbf{u}}_f(y) + S(\boldsymbol{\omega}_B + \boldsymbol{\omega}_L \\ & + \mathbf{T}_{BR}\boldsymbol{\omega}_s)\mathbf{T}_{BR}[\mathbf{u}_f + S(\boldsymbol{\omega}_s)\mathbf{r}_s] + \mathbf{T}_{BR}[S(\dot{\boldsymbol{\omega}}_s)\mathbf{r}_s]\}\,\mathrm{d}y \\ & = [\,X_B \quad Y_B \quad Z_B\,]^T \end{aligned} \tag{8}$$

where $[X_B, Y_B, Z_B]$ is the net force acting on the aircraft (aerodynamic plus gravitational), with components in the body frame. An expression for the net force is given in Sec. II.G. The position vector of the CG is given by

$$\begin{aligned} \dot{\mathbf{r}}_{\mathrm{CG}} = \frac{1}{m}\Bigg\{ & \tilde{m}_R\int_0^{b/2}[\mathbf{u}_f + S(\boldsymbol{\omega}_R)\mathbf{T}_{BR}\mathbf{y}]\,\mathrm{d}y + \tilde{m}_L\int_{-b/2}^{0}[\mathbf{u}_f \\ & + S(\boldsymbol{\omega}_L)\mathbf{T}_{BR}\mathbf{y}]\,\mathrm{d}y\Bigg\} \end{aligned} \tag{9}$$

For highly flexible or rapidly flapping wings, the dynamics of the CG serve to couple the translational and rotational dynamics tightly. The CG location can be changed using an actuated mass, such as the bob weight in Doman et al. [27], for controlling the aircraft attitude.

The total angular momentum of the aircraft is given by

$$\begin{aligned} \mathbf{h} = {} & \mathbf{J}\boldsymbol{\omega}_B + mS(\mathbf{r}_{\mathrm{CG}})\mathbf{u}_B - \int_0^{b/2}\{[S(\mathbf{T}_{BR}\mathbf{y} + \mathbf{T}_{BR}\mathbf{x})]\mathbf{u}_f + S(\mathbf{T}_{BR}\mathbf{y} \\ & + \mathbf{T}_{BR}\mathbf{x})[S(\mathbf{T}_{BR}\mathbf{y} + \mathbf{T}_{BR}\mathbf{x})(\boldsymbol{\omega}_B + \boldsymbol{\omega}_R) + S(\mathbf{T}_{BR}\mathbf{x})\boldsymbol{\omega}_s]\}\,\mathrm{d}m \\ & - \int_{-b/2}^{0}\{[S(\mathbf{T}_{BR}\mathbf{y} + \mathbf{T}_{BR}\mathbf{x})]\mathbf{u}_f + S(\mathbf{T}_{BR}\mathbf{y} + \mathbf{T}_{BR}\mathbf{x})[S(\mathbf{T}_{BR}\mathbf{y} \\ & + \mathbf{T}_{BR}\mathbf{x})(\boldsymbol{\omega}_B + \boldsymbol{\omega}_L) + S(\mathbf{T}_{BR}\mathbf{x})\boldsymbol{\omega}_s]\}\,\mathrm{d}m \end{aligned}$$

where $\mathbf{x}$ represents the coordinates of a point on the cross section of the wing in the local station frame. The moment of inertia of the right wing is given by

$$\mathbf{J}_R = -\int_0^{b/2} S^2(\mathbf{T}_{BR}\mathbf{y} + \mathbf{T}_{BR}\mathbf{x})\,\mathrm{d}m \tag{10}$$

and $\mathbf{J}_L$ is defined similarly. It follows that

$$\begin{aligned}\mathbf{h} = {} & \mathbf{J}\boldsymbol{\omega}_B + \mathbf{J}_R\boldsymbol{\omega}_R + \mathbf{J}_L\boldsymbol{\omega}_L + mS(\mathbf{r}_{\mathrm{CG}})\mathbf{u}_B - \int_0^{b/2} S(\mathbf{T}_{BR}\mathbf{y} \\ & + \mathbf{T}_{BR}\mathbf{x})\mathbf{T}_{BR}[\mathbf{u}_f + S(\mathbf{x})\boldsymbol{\omega}_s]\,\mathrm{d}m - \int_{-b/2}^{0} S(\mathbf{T}_{BR}\mathbf{y} \\ & + \mathbf{T}_{BR}\mathbf{x})\mathbf{T}_{BR}[\mathbf{u}_f + S(\mathbf{x})\boldsymbol{\omega}_s]\,\mathrm{d}m\end{aligned} \tag{11}$$

where $\rho_{w,R}$ and $\rho_{w,L}$ denote the densities of the right and left wing, respectively, and $\mathbf{J}$ is the total moment of inertia of the aircraft. The reader would be correct in judging that differentiating this expression would yield a cumbersome set of equations for the rotational dynamics. To keep the expression tractable, it has been assumed that the moment of inertia of the wing is constant in magnitude; i.e., the effect of wing bending and twist on the net moment of inertia of the aircraft is ignored. Subject to this assumption, the following dynamic equation for rotational motion is obtained:

$$\begin{aligned}& \mathbf{J}\dot{\boldsymbol{\omega}}_B + S(\boldsymbol{\omega}_B)\mathbf{J}\boldsymbol{\omega}_B + mS(\boldsymbol{\omega}_B)S(\mathbf{r}_{\mathrm{CG}})\mathbf{u}_B + mS(\mathbf{r}_{\mathrm{CG}})\dot{\mathbf{u}}_B \\ & + S(\dot{\mathbf{r}}_{\mathrm{CG}})\mathbf{u}_B + \mathbf{J}_R\dot{\boldsymbol{\omega}}_R + \mathbf{J}_L\dot{\boldsymbol{\omega}}_L + S(\boldsymbol{\omega}_B)(\mathbf{J}_R\boldsymbol{\omega}_R + \mathbf{J}_L\boldsymbol{\omega}_L) \\ & + [S(\boldsymbol{\omega}_R)\mathbf{J}_R - \mathbf{J}_RS(\boldsymbol{\omega}_R)](\boldsymbol{\omega}_B + \boldsymbol{\omega}_R) + [S(\boldsymbol{\omega}_L)\mathbf{J}_L \\ & - \mathbf{J}_LS(\boldsymbol{\omega}_L)](\boldsymbol{\omega}_B + \boldsymbol{\omega}_L) - \tilde{m}_R\int_0^{b/2}\{S(\boldsymbol{\omega}_B \\ & + \boldsymbol{\omega}_R)S(\mathbf{T}_{BR}\mathbf{y})\mathbf{T}_{BR}[\mathbf{u}_f + S(\mathbf{r}_s)\boldsymbol{\omega}_s] + S(\mathbf{T}_{BR}\mathbf{y})\mathbf{T}_{BR}[\dot{\mathbf{u}}_f \\ & + S(\mathbf{r}_s)\dot{\boldsymbol{\omega}}_s]\}\,\mathrm{d}y - \tilde{m}_L\int_{-b/2}^{0}\{S(\boldsymbol{\omega}_B + \boldsymbol{\omega}_L)S(\mathbf{T}_{BR}\mathbf{y})\mathbf{T}_{BR}[\mathbf{u}_f \\ & + S(\mathbf{r}_s)\boldsymbol{\omega}_s] + S(\mathbf{T}_{BR}\mathbf{y})\mathbf{T}_{BR}[\dot{\mathbf{u}}_f + S(\mathbf{r}_s)\dot{\boldsymbol{\omega}}_s]\}\,\mathrm{d}y \\ & + \int_0^{b/2}\{\rho_{w,R}[\mathbf{T}_{BR}\mathbf{J}_s\dot{\boldsymbol{\omega}}_s + S(\boldsymbol{\omega}_B + \boldsymbol{\omega}_R)\mathbf{T}_{BR}\mathbf{J}_s\boldsymbol{\omega}_s] \\ & - \tilde{m}_RS(\mathbf{T}_{BR}\mathbf{u}_f)\mathbf{T}_{BR}S(\mathbf{r}_s)\boldsymbol{\omega}_s\}\,\mathrm{d}y + \int_{-b/2}^{0}\{\rho_{w,L}[\mathbf{T}_{BR}\mathbf{J}_s\dot{\boldsymbol{\omega}}_s \\ & + S(\boldsymbol{\omega}_B + \boldsymbol{\omega}_L)\mathbf{T}_{BR}\mathbf{J}_s\boldsymbol{\omega}_s] - \tilde{m}_LS(\mathbf{T}_{BR}\mathbf{u}_f)\mathbf{T}_{BR}S(\mathbf{r}_s)\boldsymbol{\omega}_s\}\,\mathrm{d}y \\ & = [L \quad M \quad N]^T\end{aligned} \tag{12}$$

where $\mathbf{J}_s(y) = -\iint_S S^2(\mathbf{x})\,\mathrm{d}A$ denotes the second moment of area matrix of a cross section of the wing. An expression for the net moment ($[L \quad M \quad N]^T$) is given in Sec. II.G. Note that if the terms arising from flexibility are ignored along with the wing root angular velocity, then, with the additional assumption that $\mathbf{r}_{\mathrm{CG}} = 0$, Euler's equations are recovered as one would expect. The equations of motion derived in this paper incorporate wing rotation [see Eq. (3), which expresses $\boldsymbol{\omega}_R$ in terms of the flapping rates] and therefore this model can be used for a study of flexible flapping wings as well.

E. Structural Dynamics

The bending and twisting elastic equations of motion for the right wing are given by

$$\begin{bmatrix} \tilde{m}_R & -\tilde{m}_Rx_ec \\ -\tilde{m}_Rx_ec & I_p \end{bmatrix}\begin{bmatrix} [\dot{\mathbf{V}}]_3 \\ [\dot{\boldsymbol{\Omega}}]_2 \end{bmatrix} + \begin{bmatrix} \eta(E\tilde{I}_b\dot{\xi}'')'' + (E\tilde{I}_b\xi'')'' - T\xi'' \\ -\eta(G\tilde{J}\dot{\theta}_s')' - (G\tilde{J}\theta_s')' \end{bmatrix} = \begin{bmatrix} \mathbf{F}_{s,3} \\ \mathbf{M}_{s,2} \end{bmatrix} \tag{13}$$

where

$$\dot{\boldsymbol{\Omega}} = \dot{\boldsymbol{\omega}}_s + \mathbf{T}_{SB}(\dot{\boldsymbol{\omega}}_B + \dot{\boldsymbol{\omega}}_R) \tag{14}$$

and

$$\begin{aligned}\dot{\mathbf{V}} = {} & \mathbf{T}_{SB}\dot{\mathbf{u}}_B + \dot{\mathbf{u}}_f + S(\boldsymbol{\omega}_B + \boldsymbol{\omega}_R)(\mathbf{T}_{SB}\mathbf{u}_B + \mathbf{u}_f) + \mathbf{T}_{SB}S(\boldsymbol{\omega}_B \\ & + \boldsymbol{\omega}_R)\mathbf{T}_{BR}\mathbf{u}_f + \mathbf{T}_{SB}[S(\dot{\boldsymbol{\omega}}_B + \dot{\boldsymbol{\omega}}_R) + S^2(\boldsymbol{\omega}_B + \boldsymbol{\omega}_R)] \\ & \times \mathbf{T}_{BR}\mathbf{y} \qquad \xi = \xi_f - y\delta_R \qquad \mathbf{u}_f = [0 \quad 0 \quad \dot{\xi}_f]^T\end{aligned} \tag{15}$$

Remark: The displacement ξ should be viewed as comprising of the deformation ξ_f, and a rigid component, $y\delta_R$, i.e., $\xi = \xi_f(y) - y\delta_R$, with $\xi_f'(0) = 0$. This perspective is helpful from the point of view of practical implementation of boundary control schemes. Likewise, one may consider θ_s as the sum of flexible and rigid twist contributions (denoted by θ_R in this paper), instead of a pure deformation. Then, the wing may be viewed as being clamped at the root, with $\theta_s(0) = \theta_R + 0$ (zero deformation at the root). This decomposition of ξ and θ_s changes neither the governing equations nor the boundary conditions, because the rigid terms do not affect the stiffness and damping terms, while they are already incorporated into the accelerations and the right-hand side.

Note that $I_p = \rho_w\mathbf{J}_s(2,2)$ and $I_b = \mathbf{J}_s(1,1)$, where ρ_w denotes the density of the wing. Furthermore, $\mathbf{F}_{s,3} \triangleq \mathbf{F}_{s,3}(\alpha, \dot{\alpha}, V_\infty, \mathbf{u}_f, \theta, \dot{\theta})$ is the total force acting in the local z direction (hence the subscripts s and *3*), while $\mathbf{M}_{s,2} \triangleq \mathbf{M}_{s,2}(\alpha, \dot{\alpha}, V_\infty, \mathbf{u}_f, \theta, \dot{\theta})$ is the local pitching moment. The arguments of $\mathbf{F}$ and $\mathbf{M}$ listed here are by no means exhaustive; rather, they are the primary contributors. The term $[\dot{\mathbf{V}}]_3$ denotes the z component of the local acceleration, and $[\dot{\boldsymbol{\omega}}]_2$ is the y component of the local angular acceleration. Expressions for the net force and moment are given in Sec. II.G. The Kelvin–Voigt damping coefficient is obtained by scaling $E\tilde{I}_b$ and $G\tilde{J}$ by a factor of η in the bending and twist equations, respectively.

Remark: The scaling term η will not be equal for both cases, viz., bending and twist, in the most general case. Furthermore, it is common among structural dynamicists to model the damping coefficient as a linear combination of the mass (or moment of inertia) and stiffness.

Remark: The linear model presented here can be readily replaced by a nonlinear model in the proposed coordinates to match the requirements of the problem at hand.

The boundary conditions are given by the following expressions:

1) At the wing root: $\xi = 0$, while ξ' and θ_s can be set arbitrarily (within admissible limits) as the dihedral angle and the twist, respectively, at the wing root.

2) At the wing tip: $\xi'' = 0$, $(E\tilde{I}_b\xi'')' - T\xi' = 0$ and $\theta_s' = 0$ (i.e., free end boundary conditions).

Remark: If the tension T is spatially varying, i.e., $T \equiv T(y)$, then an additional term, $T'\xi_f'$, needs to be added alongside $T\xi''$ in Eq. (13).

Boundary conditions at the wing root, in particular $\theta_s(0)$ and $\xi'(0)$, can be controlled actively via dedicated actuators for stabilizing an unstable wing or for ensuring that the net force on the wing or its components achieve the desired value for specific maneuvers [28].

F. Fuselage Kinematics

The fuselage attitude is described by the Euler angles ψ, θ, and ϕ. The kinematic equations are given by

$$\begin{aligned}\dot{\phi} = p + q\tan\theta\sin\phi + r\tan\theta\cos\phi, \qquad \dot{\theta} = q\cos\phi - r\sin\phi \\ \dot{\psi} = (q\sin\phi + r\cos\phi)\sec\theta\end{aligned} \tag{16}$$

The equations which relate the position of the aircraft to its translational velocity are essentially decoupled from the flight dynamics, and are given by

$$\dot{X} = V_{gn}\cos\gamma\cos\chi \qquad \dot{Y} = V_{gn}\cos\gamma\sin\chi \qquad \dot{Z} = -V_{gn}\sin\gamma \tag{17}$$

where V_{gn} is the ground speed of the aircraft (obtained by subtracting the velocity of the wind from that of the aircraft). The flight-path angle (γ) and the wind axis heading angle (χ) in Eq. (17) are defined as follows:

$$\sin\gamma = \cos\alpha\cos\beta\sin\theta - \sin\beta\sin\phi\cos\theta - \sin\alpha\cos\beta\cos\phi\cos\theta$$

$$\sin\chi\cos\gamma = \cos\alpha\cos\beta\cos\theta\sin\psi + \sin\beta(\sin\phi\sin\theta\sin\psi + \cos\phi\cos\psi) + \sin\alpha\cos\beta(\cos\phi\sin\theta\sin\psi - \sin\phi\cos\psi) \quad (18)$$

The turn rate is given by $\omega = \dot{\chi}$. If $\dot{\theta} = \dot{\phi} = \dot{\beta} = 0$, it follows that

$$\omega = \dot{\psi} = (q\sin\phi + r\cos\phi)\sec\theta \quad (19)$$

G. Forces

The net force on the aircraft consists primarily of contributions from aerodynamic and gravitational forces. The aerodynamic forces and moments are computed using strip theory which is used routinely in the literature (see [1] for a summary). The wing is divided into chordwise strips. The lift, drag, and the quarter-chord aerodynamic moment at each strip can be computed by using a suitable aerodynamic model and these can be summed over the entire wing to yield the net aerodynamic force and moment. A similar calculation is performed for the horizontal tail and added to the wing contributions. The aerodynamic contributions of the fuselage are ignored with the understanding that they can be added readily to the model developed in this paper.

Since the model developed in this paper is intended to be as generic as possible, the model proposed by Goman and Khrabrov [21] is presented in this section as a candidate model for computing the lift and the quarter-chord moment while drag is estimated assuming the classic drag polar. In the authors' estimate, Goman and Khrabrov's model offers at least two advantages over the existing models (such as Theodorsen [12] or Peters et al. [29]). First, the model is cast in the form of a single ordinary differential equation (ODE) and two algebraic equations, one each for lift and the quarter-chord pitching moment. The state variable for the ODE corresponds, physically, to the chordwise location of flow separation on the airfoil. Therefore, the model is quite easy to implement as part of a numerical routine. Second, the model is inherently nonlinear and applicable to poststall flight. In particular, it captures the hysteresis in C_L due to cyclic variations in the angle of attack.

The following equation describes the movement of the separation point for unsteady flow conditions:

$$\tau_1\dot{\nu} + \nu = \nu_0(\alpha - \tau_2\dot{\alpha}) \quad (20)$$

where ν denotes the position of the separation point, τ_1 is the relaxation time constant, and τ_2 captures the time delay effects due to the flow, while ν_0 is an expression for the nominal position of the separation point. These three parameters need to be identified experimentally or using computational fluid dynamics for the particular airfoil under consideration. The coefficients of lift and quarter-chord moment are then given by

$$C_l^* = \frac{\pi}{2}\sin[\alpha(1+\nu+2\sqrt{\nu})]$$
$$C_{m_{ac}}^* = \frac{\pi}{2}\sin[\alpha(1+\nu+2\sqrt{\nu})]\left[\frac{5+5\nu-6\sqrt{\nu}}{16}\right] \quad (21)$$

and the lift and the quarter-chord moment per unit span are given by

$$L(y) = 0.5\rho V(y)^2 c C_l^* + \frac{\pi}{4}\rho c^2[\ddot{\xi} + V_\infty\dot{\alpha} - (x_a - 0.25)c\ddot{\alpha}]$$
$$M(y) = 0.5\rho V(y)^2 c^2 C_{m_{ac}}^* + \frac{\pi}{4}\rho c^2\left\{V_\infty\dot{\xi} + \frac{(x_a-0.25)c\ddot{\xi}}{2} + V_\infty^2\alpha - c^2\left[\frac{1}{32} + (x_a-0.25)^2\right]\ddot{\alpha}\right\} \quad (22)$$

where α is the local angle of attack, ρ denotes the density of air, and ξ is the transverse displacement of the wing due to the wing deformation as well as flapping. Furthermore, $V = \|\mathbf{V}\|$ is the local wind speed with $\mathbf{V}$ defined in Eq. (4), and V_∞ is the freestream speed of the aircraft given by $V_\infty = \|\mathbf{u}_B\|$. The last term of each expression was added to Goman and Khrabrov's original model [21] and corresponds to the apparent mass effect [4,23].

There is, unfortunately, no simple expression for the sectional drag coefficient. The sectional drag coefficient can be written as

$$C_d = \frac{0.89}{\sqrt{Re}} + \frac{1}{\pi e A_R}C_l^2 \quad (23)$$

where $C_l = L(y)/0.5\rho V(y)^2 c$, A_R is the aspect ratio of the wing, Re denotes the chordwise Reynolds number, and e is Oswald's efficiency factor. The skin friction term [30] assumes laminar flow over the wing and may need to be replaced with a different approximation (see DeLaurier [23] for instance). The drag model is quasi steady in nature so that dynamic stall effects are not included. A refined model for calculating drag, incorporating dynamic stall, may be found in DeLaurier [23].

The local aerodynamic force on each wing can be written in the body axis system:

$$\begin{bmatrix} X_A(y) \\ Y_A(y) \\ Z_A(y) \end{bmatrix} = \mathbf{T}_{BS}\begin{bmatrix} L(y)\sin\alpha(y) - D(y)\cos\alpha(y) \\ 0 \\ -L(y)\cos\alpha(y) - D(y)\sin\alpha(y) \end{bmatrix} \quad (24)$$

Note that $\mathbf{T}_{BS}$ is used instead of $\mathbf{T}_{BR}$ and this is the most important source of the difference between the net forces and moments on a flexible wing vis-a-vis a rigid wing. The components of the gravitational force are given by

$$X_g = -mg\sin\theta, \qquad Y_g = mg\cos\theta\sin\phi$$
$$Z_g = mg\cos\theta\cos\phi \quad (25)$$

and the corresponding moment is given by $S(\mathbf{r}_{cg})[X_g \quad Y_g \quad Z_g]^T$.

The net aerodynamic force on the two wings is given by

$$\begin{bmatrix} X_B \\ Y_B \\ Z_B \end{bmatrix}_{\text{wing}} = \int_0^{b/2}\begin{bmatrix} X_A(y) \\ Y_A(y) \\ Z_A(y) \end{bmatrix}_{\text{right}}\mathrm{d}y + \int_0^{b/2}\begin{bmatrix} X_A(y) \\ Y_A(y) \\ Z_A(y) \end{bmatrix}_{\text{left}}\mathrm{d}y \quad (26)$$

The net aerodynamic moment due to the two wings is given by

$$\begin{bmatrix} L \\ M \\ N \end{bmatrix}_{\text{wing}} = \int_0^{b/2} S(\mathbf{y})\begin{bmatrix} X_A(y) \\ Y_A(y) \\ Z_A(y) \end{bmatrix}_{\text{right}}\mathrm{d}y + \int_0^{b/2} S(\mathbf{y})\begin{bmatrix} X_A(y) \\ Y_A(y) \\ Z_A(y) \end{bmatrix}_{\text{left}}\mathrm{d}y \quad (27)$$

A similar calculation can be performed for the horizontal tail. The net force and moment on the aircraft themselves are the sum of the contributions from the wing, the horizontal tail, and gravity:

$$\begin{bmatrix} X_B \\ Y_B \\ Z_B \end{bmatrix} = \begin{bmatrix} X_B \\ Y_B \\ Z_B \end{bmatrix}_{\text{wing}} + \begin{bmatrix} X_B \\ Y_B \\ Z_B \end{bmatrix}_{\text{tail}} + \begin{bmatrix} X_g \\ Y_g \\ Z_g \end{bmatrix}$$
$$\begin{bmatrix} L \\ M \\ N \end{bmatrix} = \begin{bmatrix} L \\ M \\ N \end{bmatrix}_{\text{wing}} + \begin{bmatrix} L \\ M \\ N \end{bmatrix}_{\text{tail}} + S(\mathbf{r}_{cg})\begin{bmatrix} X_g \\ Y_g \\ Z_g \end{bmatrix} \quad (28)$$

This completes the formulation of the equations of motion.

H. Trim Equations

The rigid body equations of motion and the structural dynamic equations are coupled because of acceleration terms. Therefore, for the purpose of locating equilibrium flight conditions (or trims), the rigid body equations of motion and the structural dynamic equations can be decoupled. Specifically, the structural dynamic equations

themselves split into bending and twisting equations, which give rise to boundary value problems.

Trims are computed for the flexible winged aircraft using the fsolve routine in MATLAB. The structural mechanic boundary value problem is solved in the loop using MATLAB's built-in boundary value problem solver called bvp4c [31]. The wings are assumed to be quasi-statically deformed, which allows for stability computation of the aircraft motion using the flight dynamic equations.

III. Applications of the Model

A schematic of the aircraft model used for numerical analysis is shown in Fig. 3. An experimentally derived steady aerodynamic model [32] is employed here. This is an admissible model because the wing is assumed to be statically deformed for the purpose of trim and stability analysis. The sectional aerodynamic coefficients for lift, drag, and pitching moment are given by

$$C_l = 0.28295 + 2.00417\alpha, \qquad C_d = 0.0346 + 0.3438C_l^2$$
$$C_{m,ac} = -0.1311 \tag{29}$$

The coefficient of lift, in particular, tallies very well with predictions from thin airfoil theory. The coefficient of drag, on the other hand, is larger than the prediction of the simple formula in Eq. (23) by an order of magnitude. It is worth noting that this aerodynamic model was obtained for the Parkzone Vapor,[¶] whose geometry is identical to that of the aircraft considered in the present paper. Among other parameters, the low lift-to-drag C_L/C_D ratio is a characteristic of the Reynolds number regime of MAVs [$\mathcal{O}(1 \times 10^4)$].

A. Analysis of the Wing and Effective Dihedral

The Young's modulus of the wing, E, may be considered as a design parameter. To exploit the idea of using the wing dihedral for yaw control, the wing dihedral effect itself may be looked upon as a design driver for E.

The role of differential (or asymmetric) dihedral for yaw control has been discussed in detail in [1]. The dihedral primarily produces a side force, which is actually a component of the total force produced by the wing normal to its local plane. Let Y_A and Z_A denote the local forces produced by the wing along the body y and z axes, respectively. Therefore, one may define a term called the effective dihedral, δ_{eff}, as follows:

$$\delta_{\text{eff}} = \tan^{-1}\left(\frac{\int_0^{b/2} Y_A(y)\,\mathrm{d}y}{\int_0^{b/2} Z_A(y)\,\mathrm{d}y}\right) \tag{30}$$

This notion of the effective dihedral is different from, and arguably more general than, that of Rodden [19] who derived expressions for the increments, arising from wing bending, in the rolling moment derivatives. The notion of the effective dihedral is particularly useful for wing design from the point of view of elasticity. The Young's modulus, E, could be chosen to ensure that the wing produces a sufficient effective dihedral effect with reasonable actuator forces. The effective dihedral depends on the boundary conditions to which the wing is subjected whereas the boundary conditions themselves depend on the location and type of actuators. For a rigid wing, the effective dihedral and the actual dihedral are equal.

Figures 4a and 4b show the effective dihedral as a function of the wing dihedral angle at the root. The effective dihedral, as expected, is much higher for $E = 5$ MPa as compared to $E = 50$ MPa. In the former case, the wing bending is large enough so that flexibility provides a substantial increase in the wing dihedral effect. This suggests that for the particular wing geometry considered in this paper, a material with a Young's modulus of $E \sim \mathcal{O}(1)$ MPa should be chosen in order to obtain a significant dihedral effect. This conclusion depends on other chosen parameters and hence, such analysis should be performed on a case-by-case basis. Furthermore, it is important to note that the effective dihedral depends on the trim condition under consideration.

[¶]Data available online at http://www.parkzone.com/Products/Default.aspx?ProdID=PKZ3380 [retrieved 3 Feb. 2012].

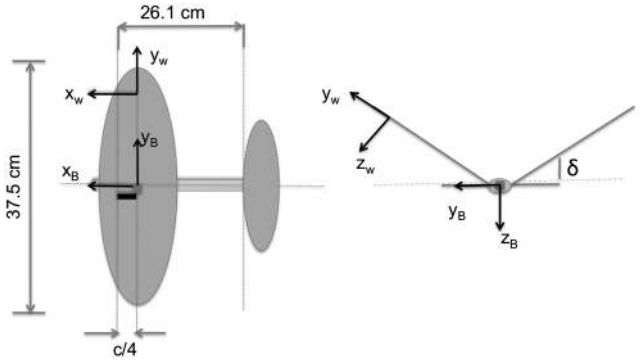

Fig. 3 A schematic showing the aircraft and the relevant dimensions. The wings can rotate about the root to supply variable twist and dihedral. The subscript w denotes a coordinate frame at an arbitrary spanwise station on the wing.

The effective dihedral is useful in another way. It forms the basis to extend the stability analysis for a rigid aircraft to the case of flexible wings. In [1], for example, analytical expressions for the traditional lateral stability derivatives were obtained for a rigid aircraft and the stability of lateral-directional modes was examined for various values of the wing dihedral. Those results would be applicable to a flexible winged aircraft when the effective dihedral angle of the wing is matched to the dihedral angle of a rigid wing. This is valid regardless of the deformation profile of the wing. For the aircraft model considered here, it suggests that the motion stability would be similar to that of the rigid aircraft when $E \geq \mathcal{O}(10)$ MPa.

B. Feasibility of Using Wing Tension

At this point, it is helpful to note a design tradeoff. A smaller E would provide a larger dihedral effect due to the aerodynamic loads on the wing. However, the same wing would be unable to generate as much anhedral because, usually, the wing would be expected to supply an upward lifting force. In principle, it seems that this limitation can be overcome by stiffening the wing internally. The effect of stiffening the wing on its effective dihedral effect is demonstrated in Fig. 5a. The three curves in the figure correspond to tensions of 0, 5, and 10 g, respectively. The Young's modulus was set to $E = 5$ MPa. The tension values were chosen to be commensurate with the weight of the aircraft, with the understanding that servos similar to those which maneuver the wing should be able to provide these values of tension. Clearly, the effective dihedral decreases substantially with tension. The effect of tension becomes less significant as the Young's modulus of the material is increased, as shown in Fig. 5b. Whereas the conclusion is quite obvious, such analysis helps choose a suitable Young's modulus for the wing.

Interestingly, stiffening the wing not only reduces the effective dihedral of the wing, but it also flattens the curve of the effective dihedral as a function of the dihedral at the wing root. Consequently, when a certain anhedral is required, the tensed wing will produce a lesser magnitude of anhedral as well.

C. Bending and Twist Natural Frequencies

Traditionally, natural frequencies of lifting surfaces are defined in terms of inertia and elastic stiffness. However, unsteady aerodynamic lift and moment relations contain terms which mathematically play the same role as stiffness, damping, and inertia in the governing relations. Consequently, another set of natural pseudo frequencies can be defined which include these aerodynamic contributions.

Consider the case where $\theta'(b/2) = \xi''(b/2) = \xi'''(b/2) = 0$. If ω_θ and ω_ξ denote the frequencies of the first (decoupled) twisting and bending modes, respectively, then it can be shown that [4]

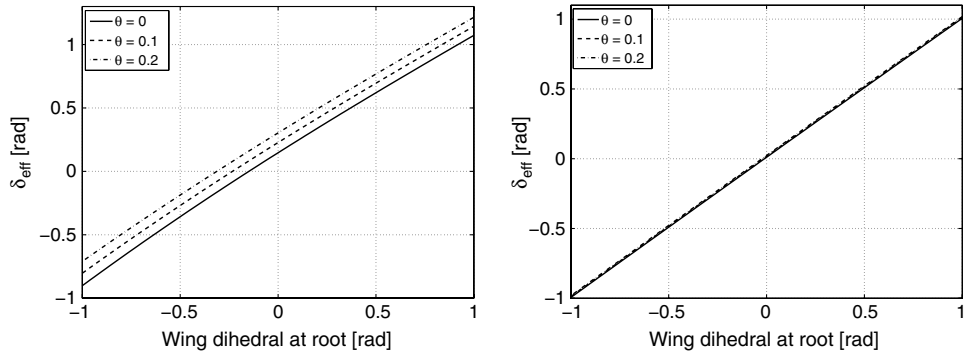

a) Effective dihedral when E = 5 MPa b) Effective dihedral when E = 50 MPa

Fig. 4 Effective dihedral as a function of the dihedral angle at the wing root for two different values of the Young's modulus. Each plot shows the effective dihedral for three values of wing tip twist θ: 0, 0.1, and 0.2 rad. This plot was obtained for $V = 2.5$ m/s and $\alpha = 10$ deg.

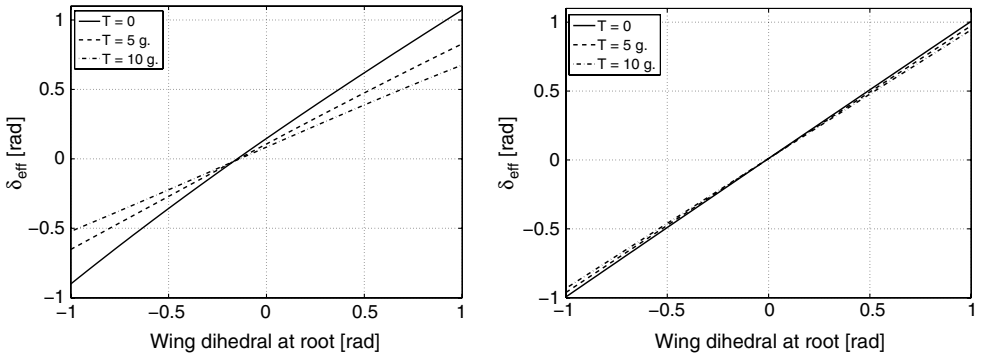

a) Effective dihedral when E = 5 MPa b) Effective dihedral when E = 50 MPa

Fig. 5 Effect of tension on the effective dihedral. The curves corresponding to a tension of 0, 5, and 10 g are plotted. The flight speed was set to $V = 2.5$ m/s, and the angle of attack was $\alpha = 10$ deg.

$$\omega_\theta^2 = \frac{\pi^2}{4L^2}\frac{G\tilde{J}}{I_p} - \frac{M}{I_p}, \qquad \omega_\xi^2 = \frac{12.36}{L^4}\frac{EI_b}{\tilde{m}}, \qquad L = b/2 \tag{31}$$

where M denotes $\partial \mathbf{M}_{s,2}/\partial\theta$ (the linearized twisting moment). The terms $\tilde{m}$ and I_p are assumed to incorporate a suitable mass of air which accounts, in part, for the unsteady effects. To estimate the extent of time scale separation, the ratio $\omega_\theta^2/\omega_\xi^2$ is of interest. Time scale separation is a property wherein the dynamics consist of two sets of modes, one of which is significantly faster than the other mode. The stability of each mode can be analyzed independently, with the other mode contributing a constant term whose value is a function of the mode being analyzed. This property is used routinely for deriving literal approximations to aircraft dynamic modes [33], and as basis for control design [34]. It must be noted that a sufficiently strong coupling between the two modes can alter the conclusions significantly. Therefore, caution must be exercised while drawing inferences from a time scale based analysis.

To estimate the ratio $\omega_\theta^2/\omega_\xi^2$, the following estimates are required: 1) $I_p \sim \mathcal{O}(\tilde{m}A_c c^2)$, where A_c is the area of cross section of the wing and $\tilde{m}$ is the density of the wing material per unit span; 2) $\tilde{J}/I_p \sim \mathcal{O}[(t_c/c)^2]/\tilde{m}$, and thus $G\tilde{J}/I_p \sim G(t_c/c)^2/\rho_w$; and 3) $I_b \sim \mathcal{O}(A_c t_c^2)$, where t_c is the wing thickness, and furthermore $\tilde{m} = \rho_w A_c$ and thus $EI_b/\tilde{m} \sim Et_c^2/\rho_w$.

From Eq. (31), it is clear that the time scale separation depends on the flight speed. It is of interest to determine the time scale separation in the absence of the M/I_p term, which is an upper bound on the time scale separation. It will closely approximate the actual time scale separation for larger values of stiffness, and would need to be scaled when the wing flexibility is increased. Ignoring the contribution from M/I_p, it follows that

$$\omega_\theta^2 \approx \frac{\pi^2}{4L^2}\frac{G\tilde{J}}{I_p} = \frac{\pi^2}{4L^2}\frac{G}{\rho_w}\frac{t^2}{c^2} \tag{32}$$

and

$$\omega_\xi^2 = \frac{12.36}{L^4}\frac{EI_b}{\tilde{m}} \approx \frac{12.36}{L^4}\frac{E}{\rho_w}\frac{t^2}{16} \tag{33}$$

where the scaling factor of 16 is obtained assuming a nearly elliptical cross section. Therefore, the ratio $\omega_\theta^2/\omega_\xi^2$ is given by

$$\frac{\omega_\theta^2}{\omega_\xi^2} \approx 3\frac{G}{E}\frac{L^2}{c^2} \approx \frac{3}{2(1+\nu_p)}\frac{L^2}{c^2} \tag{34}$$

where ν_p is Poisson's ratio. The ratio $1.5/(1+\nu_p) \approx 1$. Thus, $\omega_\theta/\omega_\xi \approx \mathcal{O}(L/c)$. Therefore, the twist dynamics are faster than the bending dynamics. The time scale separation reduces with decreasing E and increasing V, as the influence of the aerodynamic terms increasingly dominates the contribution from elasticity. The time scale separation increases with increasing aspect ratio. Although this time scale separation cannot be used to draw any inference about the susceptibility of the wing to flutter, it can be used as the basis for designing independent controllers for controlling wing bending and torsion.

D. Bifurcation Analysis of Turning Flight

The performance and stability of an MAV equipped with flexible wings ($E = 5$ MPa) in steady turning flight is analyzed in a manner similar to that described for a rigid aircraft in [1]. A similar analysis could be repeated for other maneuvers of interest. Insofar as turning is concerned, wing flexibility may have one or more of several possible consequences: 1) the overall turn rate may improve because

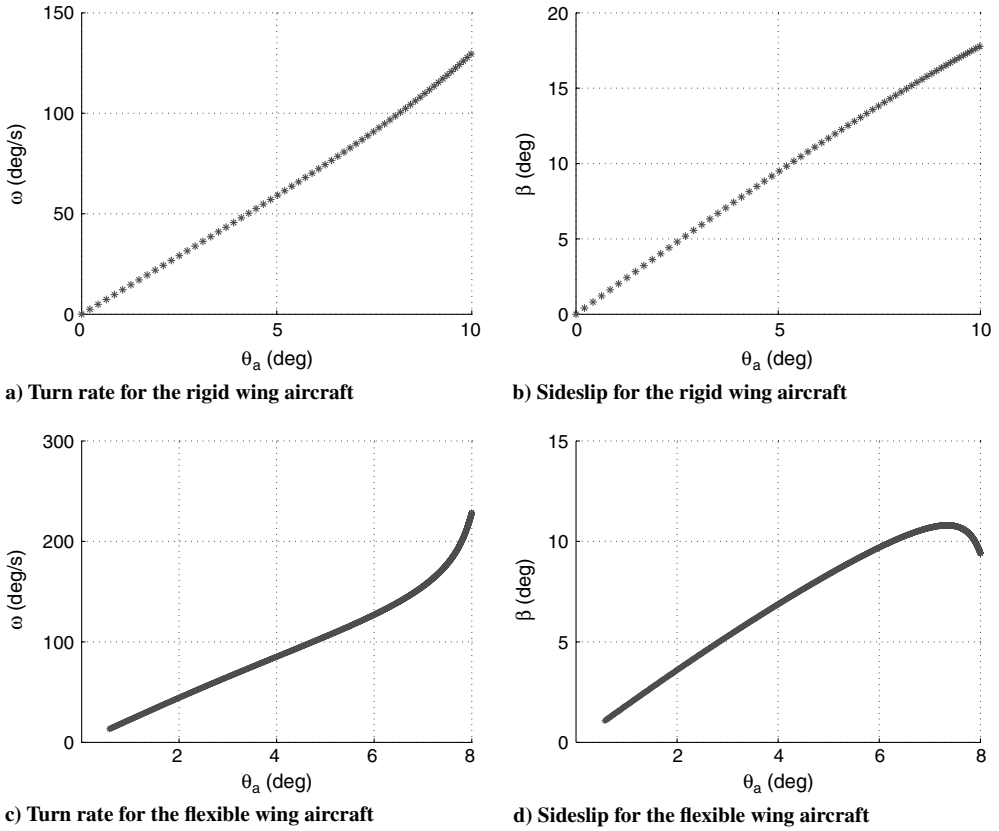

a) Turn rate for the rigid wing aircraft **b) Sideslip for the rigid wing aircraft**

c) Turn rate for the flexible wing aircraft **d) Sideslip for the flexible wing aircraft**

Fig. 6 A comparison of the sideslip and turn rate as functions of antisymmetric wing twist for otherwise identical airframes equipped with rigid and flexible wings. The wings have a Young's modulus of 5 MPa. The equilibria are marked with an asterisk to denote that the Jacobian has a single positive real eigenvalue. In both cases, the dihedral angle at both wing roots was set to 25 deg. The flight speed was set to 2.8 m/s, the elevator was fixed at -11 deg, and $\delta_L = \delta_R = 29$ deg (0.5 rad).

of the additional dihedral generated by the flexible wings; 2) alternately, for a given turn rate, the dihedral angles required at the wing root would be reduced; and 3) when the sideslip is not deliberately regulated, it would be reduced due to the enhanced dihedral effect.

It turns out that flexibility does result in a net improvement in the turn rate of the aircraft, but only when wing incidence angle at the root (or wing twist in general) is used actively. There is a significant reduction in the sideslip when the wings are locked in a symmetric dihedral configuration. However, when the dihedral angles alone are used for turns, the maximum achievable turn rate does not improve vis-a-vis a rigid aircraft. Furthermore, the magnitude of the commanded dihedral deflections required for a given turn rate is reduced in comparison to an aircraft with rigid wings.

1. Reduction in Sideslip (Variable θ_L; $\theta_R = -\theta_L = -\theta_a$; $\delta_L = \delta_R$)

A turn is usually initiated by rolling the aircraft to the appropriate bank angle and sustained by providing the appropriate yaw rate and pitch rate. When the flexible wings are twisted asymmetrically, the resultant roll rate causes a buildup in yaw rate due to the dihedral effect. However, if the wings are locked in a symmetric dihedral configuration, the resultant turn is accompanied by a sideslip which increases with increasing turn (roll) rate. This phenomenon has been

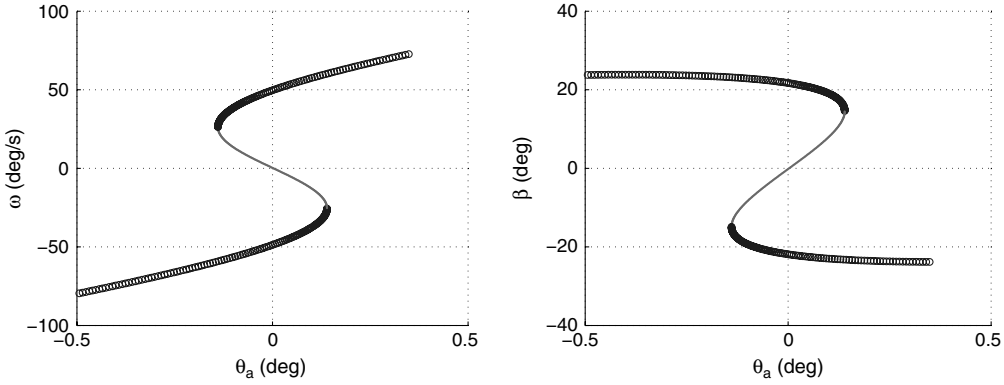

a) Turn rate **b) Sideslip**

Fig. 7 Turn rate and sideslip as functions of antisymmetric wing twist when the $\delta_L = \delta_R = 0$. Empty circles denote equilibria where the Jacobian has a pair of complex conjugate eigenvalues with positive real parts, while dots denote equilibria where the Jacobian has three eigenvalues with positive real parts: one real and a complex conjugate pair. The Young's modulus was set to $E = 5$ MPa. The flight speed was set to 2.8 m/s. The elevator deflection was set to -11 deg.

captured in Fig. 6 where the dihedral angle at the root was set to 29 deg (0.5 rad) for both wings. The equilibrium points are marked with an asterisk, indicating that they are unstable with positive real eigenvalues. For a rigid wing, the sideslip remains less than 5 deg until the turn rate builds up to 35 deg/s (compared with nearly 70 deg/s for flexible wings). Thereafter, the aerodynamic data used in this paper are insufficient to provide accurate trim results. In general, though, the sideslip increases with increasing turn rate for an aircraft with a rigid wing. On the other hand, when the wings are flexible, the turn rate increases sharply with increasing wing twist and furthermore, the sideslip peaks at just over 10 deg and drops thereafter due to the increasing effective dihedral angle. With aerodynamic data that are accurate for larger values of sideslip, the value of sideslip at the peak is liable to shift from that obtained with the present model. However, the peak itself occurs due to a favorable yawing moment which comes with an increasing wing dihedral. Therefore, a peak would be expected even with improved aerodynamic data, unless adverse yawing moment from the fuselage causes the sideslip to keep increasing with the turn rate.

It is of interest to note that the topology of the equilibrium surface depends strongly on the wing dihedral. If the root dihedral angles are set to zero, a qualitatively different picture emerges, as shown in Fig. 7. Empty circles denote equilibria where the Jacobian has a pair of complex conjugate eigenvalues with positive real parts, while dots denote equilibria where the Jacobian has three eigenvalues with positive real parts: one real and a complex conjugate pair.

The turn rate builds up rapidly and in a direction opposite to that observed in Fig. 6. Thereafter, the equilibrium curve turns around on itself at a saddle node bifurcation (the point of intersection of segments marked by dots and circles). The turn rate continues to increase while the sideslip value changes relatively slowly thereafter. Physically, this suggests that an uncontrolled aircraft will enter an oscillatory spinlike motion when the root dihedral is set to zero. Moreover, even if the equilibria are stabilized using a controller, the sign of the initial turn rate would be opposite to that observed for larger values of the root dihedral. This open-loop behavior needs to be understood thoroughly before a turning controller is designed.

2. *Coordinated Turn ($\theta_L = \theta_R = 0$; δ_L, δ_R Variable)*

The turning performance an aircraft equipped with rigid wings is compared in Fig. 8 with that of an aircraft equipped with flexible wings having Young's modulus $E = 5$ MPa. The sideslip is regulated to $\beta = 0$. The twist angle at each wing root is set to zero, i.e., $\theta_R = \theta_L = 0$. It is clear that there is actually a deterioration in the maximum achievable turn rate when the wings are flexible. However, a noticeably smaller dihedral deflection is required at the wing root for a given turn rate when the wings are flexible, as expected. The stability characteristics seen for the two sets of aircraft are identical. The points marked A, B, C, and D are all Hopf bifurcations. Evidently, none of the computed equilibria possess inherent stability.

Remark: It was seen in Sec. III.D.1 that the turn rate improved for a flexible wing MAV, accompanied by a reduced sideslip. On the other hand, in the present section, there is a deterioration in the coordinated turn performance, measured by the maximum turn rate, when the wings are flexible. This can be explained as follows. At the angle of attack considered here, the wing twists upward (i.e., the leading edge goes up) so that the net angle of attack on the wing is higher than in the rigid case. Therefore, for a given tail setting, the aircraft flies at a lower flight speed to maintain trim in pitch. The reduced speed leads to a reduction in the net lift, which, in turn, reduces the amount of centripetal force available to sustain rapid turns. Another point worth noting is that the maximum achievable turn rate depends on the maximum achievable yawing moment. The yawing moment for a given wing incidence setting reaches a maximum when the wing dihedral angle is 45 deg, or when the effective dihedral of a flexible

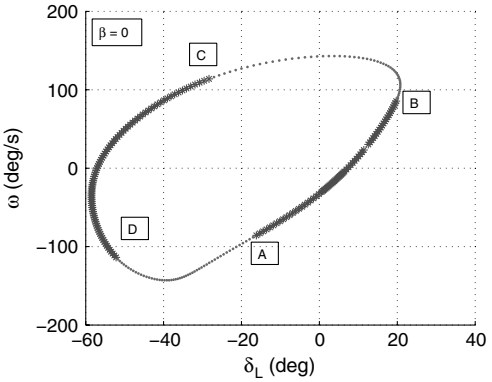

a) Turn rate for the rigid wing aircraft

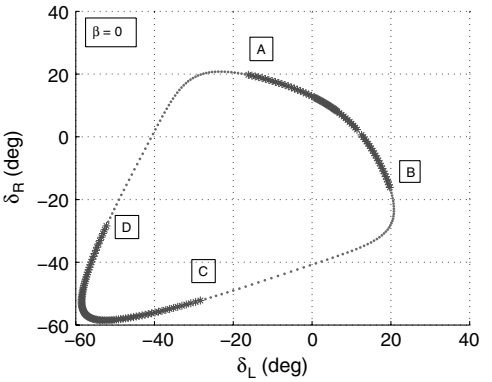

b) Right wing dihedral angle for the rigid wing aircraft

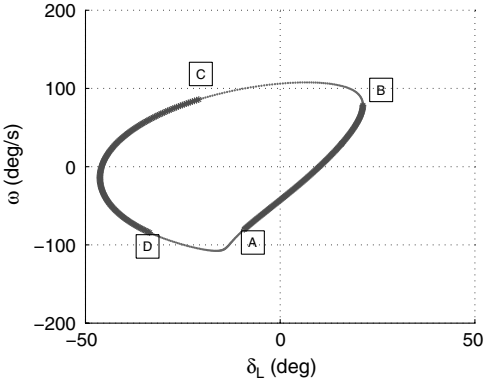

c) Turn rate for the flexible wing aircraft

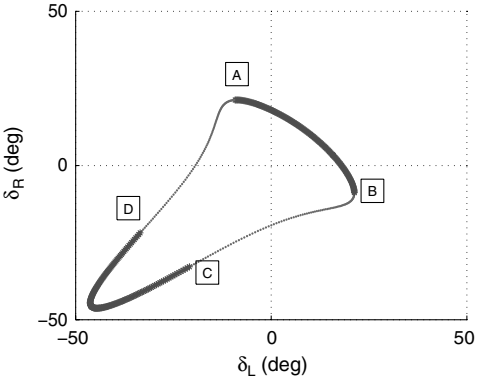

d) Right wing dihedral angle for the flexible wing aircraft

Fig. 8 A comparison of the turn rate as a function of the left wing dihedral angle, and the right wing dihedral angle required to maintain zero sideslip, for otherwise identical airframes equipped with rigid and flexible wings. In both cases, the elevator deflection was fixed at -11 deg, and $\theta_R = \theta_L = 0$. The flexible wings have a Young's modulus of 5 MPa. The Jacobian of equilibria marked by pink dots have three eigenvalues with positive real parts: one real and a complex conjugate pair. The flight speed and angle of attack are within the range of validity of the aerodynamic data.

wing equals 45 deg. This sets another fundamental limitation on the maximum achievable turn rate, and one that arises solely out of the use of wing dihedral for turning.

E. Discussion

The results presented previously yield some interesting design pointers. The wing flexibility can be reduced up to $\mathcal{O}(10)$ MPa without achieving a substantial improvement in the coordinated turn rate or any measurable change in the effective dihedral angle, although a considerable saving in the wing mass can be achieved by allowing its stiffness to reduce. The motion stability (notwithstanding the structural stability of the wing) will not be markedly different from that of a rigid configuration. One interpretation which follows is that flexibility offers only a limited improvement in the performance, notwithstanding savings on the wing mass. Alternately, a complete aeroelastic analysis can be bypassed as long as the flutter and divergence speeds are considerably larger than the prescribed flight speeds (see Sec. III.C).

These conclusions are, by no means, universally valid but, when used judiciously, can achieve considerable savings in the computational effort invested in the design. In a recent paper, Baghdadi et al. [18] observed that the open-loop stability characteristics did not change markedly between the rigid and flexible configurations considered in their paper. This is in keeping with the observations in this paper. Nevertheless, a control law designed using a rigid model yielded markedly different closed-loop stability characteristics when the time constants of the rigid and flexible modes were close to each other. On similar lines, Merrett and Hilton [35] demonstrated that flutter (motion instabilities) can arise in high-speed aircraft due to transient maneuvers such as accelerations or rapid, instantaneous turns.

IV. Conclusions

In this paper, the flight dynamics and the steady-state performance of an agile MAV equipped with flexible wings whose dihedral and twist were used as control inputs for maneuvers were described. The concept of the effective wing dihedral was introduced to decide the extent of wing flexibility required to obtain visible performance improvements over a rigid wing. Axial tension, although a promising candidate as a wing stiffener, was shown to be of limited use insofar as improving the wing anhedral was concerned. A complete aeroelastic model was derived incorporating the flexible dynamics of the wing and variable CG location. A limited version of this model, restricted to quasi-statically deformed wings, was used to compare the steady-state turning performance of the MAV with one equipped with rigid wings. It was seen that the maximum achievable turn rate improved when wing twist was used as the control input and the aircraft sideslip was not constrained. On the other hand, when the wing dihedral alone was used as the control input, a smaller control deflection was required, although there was a deterioration in the maximum achievable turn rate. Based on their observations, the authors make a twofold conclusion: 1) the wing has to be highly flexible to yield measurable performance improvements and 2) for moderately flexible wings a rigid wing model yields a sufficiently close estimate of performance and stability. Therefore, future work should focus on improving the structural model of the wing to accommodate highly flexible wings and on developing the computational tools accordingly.

Acknowledgments

This project was supported by the Air Force Office of Scientific Research under the Young Investigator Award Program (grant no. FA95500910089) monitored by Willard Larkin. The original problem was posed by Gregg Abate [Air Force Research Laboratory (AFRL)]. This paper also benefitted from stimulating discussions with Johnny Evers (AFRL).

References

[1] Paranjape, A. A., Chung, S.-J., and Selig, M. S., "Flight Mechanics of a Tailless Articulated Wing Aircraft," *Bioinspiration and Biomimetics*, Vol. 6, No. 026005, 2011. doi:10.1088/1748-3182/6/2/026005

[2] Chung, S.-J., and Dorothy, M., "Neurobiologically Inspired Control of Engineered Flapping Flight," *Journal of Guidance, Control, and Dynamics*, Vol. 33, No. 2, 2010, pp. 440–453. doi:10.2514/1.45311

[3] Paranjape, A. A., Kim, J., Gandhi, N., and Chung, S.-J., "Experimental Demonstration of Perching by a Tailless Articulated Wing MAV," AIAA Guidance, Navigation, and Control Conference, AIAA Paper 2011-6403, Portland, OR, 2011.

[4] Bisplinghoff, R. L., Holt, A., and Halfman, R. L., *Aeroelasticity*, 1st ed., Dover, Mineola, NY, 1996, pp. 421–427, 527–544, Chaps. 8, 9.

[5] Dowell, E. H., *A Modern Course in Aeroelasticity*, 4th ed., Kluwer Academic, Norwell, MA, 2004, Chaps. 2, 3.

[6] Bourdin, P., Gatto, A., and Friswell, M., "Aircraft Control via Variable Cant-Angle Winglets," *Journal of Aircraft*, Vol. 45, No. 2, 2008, pp. 414–423. doi:10.2514/1.27720

[7] Tran, D., and Lind, R., "Parametrizing Stability Derivatives and Flight Dynamics with Ding Deformation," AIAA Atmospheric Flight Mechanics Conference, AIAA Paper 2010-8227, 2010.

[8] Chakravarthy, A., Paranjape, A. A., and Chung, S.-J., "Control Law Design for Perching an Agile MAV with Articulated Wings," AIAA Atmospheric Flight Mechanics Conference, AIAA Paper 2010-7934, 2010.

[9] Stanford, B., Abdulrahim, M., Lind, R., and Ifju, P., "Investigation of Membrane Actuation for the Roll Control of a Micro Air Vehicle," *Journal of Aircraft*, Vol. 44, No. 3, 2007, pp. 741–749. doi:10.2514/1.25356

[10] Waszak, M. R., and Schmidt, D. K., "Flight Dynamics of Aeroelastic Vehicles," *Journal of Aircraft*, Vol. 25, No. 6, 1988, pp. 563–571. doi:10.2514/3.45623

[11] Meirovitch, L., and Tuzcu, I., "Unified Theory for the Dynamics and Control of Maneuvering Flexible Aircraft," *AIAA Journal*, Vol. 42, No. 4, 2004, pp. 714–727. doi:10.2514/1.1489

[12] Theodorsen, T., "General Theory of Aerodynamic Instability and the Mechanism of Flutter," NACA Rept. 496, 1935.

[13] Nguyen, N., and Tuzcu, I., "Flight Dynamics of Flexible Aircraft with Aeroelastic and Inertial Force Interactions," AIAA Atmospheric Flight Mechanics Conference, AIAA Paper 2009-6045, Chicago, 2009.

[14] Patil, M. J., and Hodges, D. H., "Flight Dynamics of Highly Flexible Flying Wings," *Journal of Aircraft*, Vol. 43, No. 6, 2006, pp. 1790–1798. doi:10.2514/1.17640

[15] Raghavan, B., and Patil, M. J., "Flight Dynamics of High-Aspect-Ratio Flying Wings: Effect of Large Trim Deformation," *Journal of Aircraft*, Vol. 46, No. 5, 2009, pp. 1808–1812. doi:10.2514/1.36847

[16] Shearer, C. M., and Cesnik, C. E. S., "Nonlinear Flight Dynamics of Very Flexible Aircraft," *Journal of Aircraft*, Vol. 44, No. 5, 2007, pp. 1528–1545. doi:10.2514/1.27606

[17] Su, W., and Cesnik, C. E. S., "Nonlinear Aeroelasticity of a Very Flexible Blended-Wing-Body Aircraft," *Journal of Aircraft*, Vol. 47, No. 5, 2010, pp. 1539–1553. doi:10.2514/1.47317

[18] Baghdadi, N., Lowenberg, M. H., and Isikveren, A. T., "Analysis of Flexible Aircraft Dynamics Using Bifurcation Methods," *Journal of Guidance, Control, and Dynamics*, Vol. 34, No. 3, 2011, pp. 795–809. doi:10.2514/1.51468

[19] Rodden, W. P., "Dihedral Effect of a Flexible Wing," *Journal of Aircraft*, Vol. 2, No. 5, 1965, pp. 368–373. doi:10.2514/3.59245

[20] Paranjape, A. A., and Ananthkrishnan, N., "Combat Aircraft Agility Metrics: A Review," *Journal of Aerospace Sciences and Technologies*, Vol. 58, No. 2, 2006, pp. 1–16.

[21] Goman, M., and Khrabrov, A., "State-Space Representation of Aerodynamic Characteristics of an Aircraft at High Angles of Attack," *Journal of Aircraft*, Vol. 31, No. 5, 1994, pp. 1109–1115. doi:10.2514/3.46618

[22] Shyy, W., Aono, H., Chimakurthi, S. K., Trizila, P., Kang, C.-K., Cesnik, C. E. S., and Liu, H., "Recent Progress in Flapping Wing Aerodynamics and Aeroelasticity," *Progress in Aerospace Sciences*, Vol. 46, No. 7, 2010, pp. 284–327.

doi:10.1016/j.paerosci.2010.01.001
[23] DeLaurier, J. D., "An Aerodynamic Model for Flapping-Wing Flight," *The Aeronautical Journal*, Vol. 97, No. 964, 1993, pp. 125–130.
[24] Larijani, R. F., and DeLaurier, J. D., "A Nonlinear Aeroelastic Model for the Study of Flapping Wing Flight," *Fixed and Flapping Wing Aerodynamics for Micro Aerial Vehicle Applications*, edited by T. J. Mueller, AIAA, Reston, VA, 2001, pp. 399–428.
[25] Bolender, M. A., "Rigid Multi-Body Equations-of-Motion for Flapping Wing MAVs using Kanes Equations," AIAA Guidance, Navigation and Control Conference, AIAA Paper 2009-6158, Chicago, 2009.
[26] Paranjape, A. A., Sinha, N. K., and Ananthkrishnan, N., "Use of Bifurcation and Continuation Methods for Aircraft Trim and Stability Analysis: A State-of-the-Art," *Journal of Aerospace Sciences and Technologies*, Vol. 60, No. 2, 2008, pp. 1–12.
[27] Doman, D., Oppenheimer, M., and Sigthorsson, D., "Wingbeat Shape Modulation for Flapping-Wing Micro-Air-Vehicle Control During Hover," *Journal of Guidance, Control, and Dynamics*, Vol. 33, No. 3, 2010, pp. 724–739.
doi:10.2514/1.47146
[28] Paranjape, A. A., Chung, S.-J., and Krstic, M., "PDE Boundary Control for Flexible Articulated Wings on a Robotic Aircraft," *IEEE Transactions on Robotics* (submitted for publication).
[29] Peters, D. A., Karunamoorthy, S., and Cao, W. M., "Finite State Induced Flow Models Part 1: Two-Dimensional Thin Airfoil," *Journal of Aircraft*, Vol. 32, No. 2, 1995, pp. 313–322.
doi:10.2514/3.46718
[30] Kuethe, A. M., and Chow, C.-Y., *Foundations of Aerodynamics*, 4th ed., Wiley, New York, 1986, p. 325.
[31] Shampine, L. F., Reichelt, M. W., and Kierzenka, J., "Solving Boundary Value Problems for Ordinary Differential Equations with bvp4c," http://www.mathworks.com/bvp_tutorial [retrieved 3 Feb. 2012].
[32] Uhlig, D., Sareen, A., Sukumar, P., Rao, A., and Selig, M., "Determining Aerodynamic Characteristics of a Micro Air Vehicle Using Motion Tracking," AIAA Atmospheric Flight Mechanics Conference, AIAA Paper 2010-8416, 2010.
[33] Ananthkrishnan, N., and Unnikrishnan, S., "Literal Approximations to Aircraft Dynamic Modes," *Journal of Guidance, Control, and Dynamics*, Vol. 24, No. 6, 2001, pp. 1196–1203.
doi:10.2514/2.4835
[34] Wang, Q., and Stengel, R. F., "Robust Nonlinear Flight Control of a High-Performance Aircraft," *IEEE Transactions on Control Systems Technology*, Vol. 13, No. 1, 2005, pp. 15–26.
doi:10.1109/TCST.2004.833651
[35] Merrett, C. C., and Hilton, H. H., "Influences of Starting Transients, Aerodynamic Definitions and Boundary Conditions on Elastic and Viscoelastic Wing and Panel Flutter," *Mathematics in Engineering, Science, and Aerospace*, Vol. 2, No. 2, 2011, pp. 121–144.

B. Epureanu
Associate Editor